The crossover conformational shift of the GTPase atlastin provides the energy driving ER fusion

James Winsor, David D. Hackney, and Tina H. Lee

Department of Biological Sciences, Carnegie Mellon University, Pittsburgh, PA 15213

The homotypic fusion of endoplasmic reticulum membranes is catalyzed by the atlastin GTPase. The mechanism involves trans-dimerization between GTPase heads and a favorable crossover conformational shift, catalyzed by GTP hydrolysis, that converts the dimer from a "prefusion" to "postfusion" state. However, whether crossover formation actually energizes fusion remains unclear, as do the sequence of events surrounding it. Here, we made mutations in atlastin to selectively destabilize the crossover conformation and used fluorescence-based kinetic assays to analyze the variants. All variants underwent dimerization and crossover concurrently, and at wild-type rates. However, certain variants were unstable once in the crossover dimer conformation, and crossover dimer stability closely paralleled lipid-mixing activity. Tethering, however, appeared to be unimpaired in all mutant variants. The results suggest that tethering and lipid mixing are catalyzed concurrently by GTP hydrolysis but that the energy requirement for lipid mixing exceeds that for tethering, and the full energy released through crossover formation is necessary for fusion.

Introduction

The substantial energy barriers that prevent spontaneous lipid bilayer fusion allow for the formation and maintenance of distinct subcellular compartments in eukaryotic cells. However, controlled fusion of these compartments must also regularly occur and so cells maintain several fusion catalysts that overcome these barriers. Fusion catalysts are typically integral membrane proteins that induce fusion by promoting the close apposition of opposing membrane bilayers and destabilizing the bilayers sufficiently to favor formation of the nonbilayer intermediates necessary for lipid mixing and membrane merger (Tamm et al., 2003; Cohen and Melikyan, 2004; Frolov and Zimmerberg, 2010; Kozlov et al., 2010).

Currently, the two best-understood types of fusion catalysts are the viral fusion proteins, which mediate fusion between viral and host cell membranes during viral entry (Skehel and Wiley, 2000; Eckert and Kim, 2001; Weissenhorn et al., 2007), and the SNARE (soluble *N*-ethyl-maleimide–sensitive fusion protein attachment protein receptor) proteins, which mediate vesicle trafficking within the secretory and endocytic pathways (Chen and Scheller, 2001; Jahn and Scheller, 2006; Südhof and Rothman, 2009). Initially, viral fusion proteins reside solely in the viral membrane but then undergo a conformational rearrangement to insert into the host membrane, thus spanning the two membranes. In contrast, SNARE fusion begins with two separate entities each stably bound to the vesicle and target, with initial trans contacts forming a complex that spans both membranes. At first glance, these two evolutionarily unrelated types of fusion catalysts appear to use differing strategies. However, after initial contact, close mechanistic parallels can be drawn (Söllner, 2004). Both undergo a series of highly favorable conformational rearrangements (Skehel and Wiley, 2000; Chen and Scheller, 2001; Eckert and Kim, 2001; Jahn and Scheller, 2006; Weissenhorn et al., 2007; Südhof and Rothman, 2009), whose energy is estimated sufficient to overcome the 40–50 k_BT energy barriers that hinder spontaneous membrane fusion (Carr et al., 1997; Kuzmin et al., 2001; Fasshauer et al., 2002; Markin and Albanesi, 2002; Yersin et al., 2003; Cohen and Melikyan, 2004; Liu et al., 2006; Li et al., 2007; Gao et al., 2012). By the end, each reaches a final stable conformation that can only exist in postfusion membranes (Sutton et al., 1998; Weissenhorn et al., 1998, 1999; Stein et al., 2009). In both of these cases, the driving force for membrane fusion comes from the highly favorable protein–protein interactions that convert the catalyst from a "prefusion" to "postfusion" state.

In the past several years, a new type of fusion protein has come under increasing study: the dynamin-related integral membrane protein atlastin responsible for the homotypic fusion of ER membranes (Park and Blackstone, 2010; McNew et al., 2013). Structurally, atlastin is distinct from either of the previously studied fusion proteins. At the N terminus, it contains a globular GTPase head domain that directly couples GTP hydrolysis to fusion activity (Orso et al., 2009). The GTPase head, also likely the site of initial trans contacts between atlastin dimers on

Correspondence to Tina H. Lee: thl@andrew.cmu.edu

Abbreviations used: 3HB, three-helix bundle; BMOE, bismaleimidoethane; CFP, cyan fluorescent protein; DATL, *Drosophila melanogaster* atlastin; FRET, Förster resonance energy transfer; hATL1, human atlastin 1; MB, Marina blue; MTS, methanethiosulfonate; NBD, nitrobenzoxadiazole; PIFE, protein-induced fluorescence enhancement; TM, transmembrane.

The Rockefeller University Press $30.00
J. Cell Biol. Vol. 216 No. 5 1321–1335
https://doi.org/10.1083/jcb.201609071

opposing ER membranes, is connected via a short linker to a fully folded three-helix bundle (3HB; Bian et al., 2011; Byrnes and Sondermann, 2011), which is in turn anchored to the ER membrane by two closely spaced trans-membrane (TM) helices. Emerging from the membrane is a C-terminal tail containing an amphipathic helix with a propensity to insert into the lipid bilayer (Liu et al., 2012; Faust et al., 2015).

Atlastin also appears to undergo highly favorable structural rearrangements between what have been termed pre- and postfusion conformations by analogy to previously studied fusion catalysts. In the so-called prefusion state, observed in the form 2 crystal structure of human atlastin1 (hATL1), two atlastin monomers interact in a head-to-head fashion with the 3HBs packed against their respective heads and pointed away from the dimer interface (Bian et al., 2011; Byrnes and Sondermann, 2011). With an interfacial binding area of only 756 Å^2, this extended dimer conformation could represent an initial encounter complex between atlastins in opposing membranes. A similar head-to-head configuration is present in the so-called postfusion state observed in the form 3 hATL1 crystal structure, though the interfacial area between heads (1,886 Å^2) is more than twice that in the form 2 prefusion dimer (Byrnes et al., 2013). A more dramatic difference in the postfusion state is that the 3HBs have been dislodged from their respective heads and are crossed over one another and with respect to the heads, having undergone a rigid body rotation about a central conserved proline residue in the linker. In the postfusion state, the close parallel alignment between 3HBs and the additional new contacts formed between the 3HBs and opposing heads creates a highly stable crossover dimer configuration with a substantial total interfacial binding area of 3,852 Å^2 (Bian et al., 2011; Byrnes and Sondermann, 2011; Byrnes et al., 2013). Though the TM domains are not present in the structures, it is hard to envision how the two molecules could adopt the postfusion conformation while remaining in separate membranes (Bian et al., 2011; Byrnes and Sondermann, 2011; Byrnes et al., 2013).

With their focus on the similarities with other fusion proteins, initial models for atlastin-catalyzed fusion had formation of the crossover conformer as the most likely source of energy for overcoming the barriers to fusion (Bian et al., 2011; Daumke and Praefcke, 2011). In those models, atlastin monomers were typically depicted to encounter one another in trans in the GTP-bound state. Thereafter, hydrolysis of the GTP would induce a series of conformational changes that would not only tighten the head-to-head binding interface but also cause expulsion of the 3HBs from their respective heads. The 3HBs, now unconstrained, would be free to undergo a rigid body rotation culminating in formation of the crossover state (Byrnes et al., 2013), which would drive lipid mixing and fusion.

Additional studies, however, reveal further complexity to the fusion mechanism. A peptide that corresponds to the atlastin tail amphipathic helix inserts into membranes and destabilizes the bilayer, whereas mutations in atlastin that inhibit this insertion block lipid mixing, showing that the tail is critically involved in the fusion process (Moss et al., 2011; Liu et al., 2012; Faust et al., 2015). Furthermore, even conservative amino acid substitutions in the TM domain block lipid mixing, though the underlying cause is not known (Liu et al., 2012). Finally, kinetic analysis of GTP-catalyzed conformational changes within the soluble domain of hATL1 has suggested head-to-head dimerization and crossover to be catalyzed concurrently by GTP hydrolysis (Byrnes et al., 2013). Collectively, these observations have been interpreted through a different type of model in which atlastins on opposing membranes come together essentially already in a crossover-like state, with the crossover conformation serving as an initial tethering unit holding opposing membranes closely together, whereas subsequent membrane insertion of the tail amphipathic helix in conjunction with the TM domains carry out the work of membrane fusion (Byrnes et al., 2013). In this alternate model, the energy released on crossover formation might play a less critical role in fusion catalysis.

Here, we set out to test the importance of atlastin's crossover conformation for membrane fusion. We reasoned that if the binding energy of the crossover conformation plays a critical role in fusion catalysis, then atlastin's fusion capacity should be exquisitely sensitive to progressive reductions in that binding energy. As a test, we generated a panel of localized point mutations within atlastin that might variably reduce, but not abolish, the stability of the crossover conformation. The effects of these mutations on crossover were assessed kinetically and their effects on atlastin's tethering and fusion activity determined. All mutant variants underwent crossover at rates indistinguishable from the wild type. On the other hand, crossover dimer stability differed widely among mutant variants, with the reduction in dimer stability closely paralleling the reduction in fusion activity, demonstrating for the first time the close coupling between the binding energy of the crossover conformation and fusion. Additionally, we observed concurrent head-to-head dimerization and crossover, confirming that tethering and fusion are triggered simultaneously by GTP hydrolysis (Byrnes et al., 2013). However, tethering was not noticeably impaired by destabilization of the crossover dimer, indicating a lower energy barrier for tethering than for fusion. Finally, the GTPase reaction rate was sensitive to the concentration of atlastin, consistent with the hydrolysis cycle depending, in some way, on dimerization. Together, the results are consistent with a model of the atlastin fusion mechanism in which GTP hydrolysis within the trans dimer triggers the concerted formation of a tightly bound crossover dimer state. If the energy released through formation of this postfusion state is sufficient to mix the lipid bilayers, then fusion ensues; otherwise, the reaction does not progress beyond tethering.

Results

Validation of a PIFE assay for crossover

Assays for atlastin crossover have largely been based on the close proximity and parallel alignment of the 3HBs occurring exclusively in the crossover conformation (Morin-Leisk et al., 2011; Byrnes et al., 2013; Saini et al., 2014; Liu et al., 2015). We previously engineered a cysteine residue (G343C) in the 3HB of the soluble domain (aa 1–415) of *Drosophila melanogaster* atlastin cytoplasmic domain (cytoDATL), and as anticipated based on the proximity of the 3HBs in the form3 hATL1 postfusion crystal structure (Byrnes et al., 2013), a homobifunctional cross-linker with a short 8 Å spacer arm conjugated two 3HBs only under conditions of crossover (Morin-Leisk et al., 2011; Saini et al., 2014). More recently, Förster resonance energy transfer (FRET) between cyan fluorescent protein (CFP) and yellow fluorescent protein (YFP) fused C-terminally to the 3HB of the hATL1 soluble domain (cyto-hATL1 CFP/YFP) has been used to establish the kinetics of crossover under stopped flow conditions (Byrnes et al., 2013). Here, as an alternate to

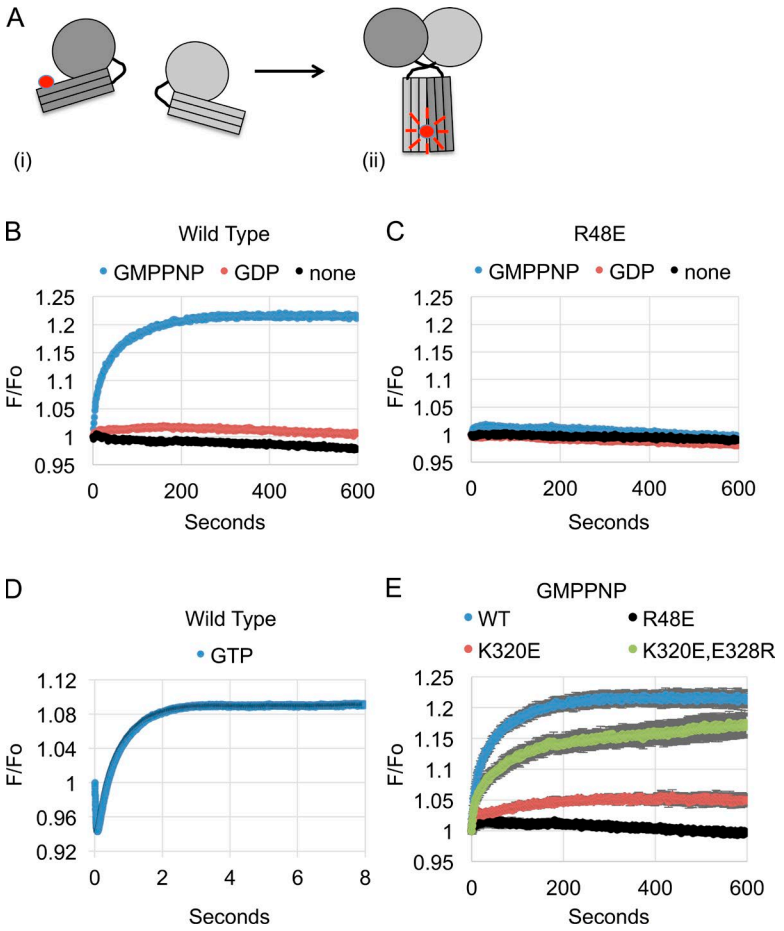

Figure 1. **PIFE assay for crossover.** (A) A schematic of Cy3 fluorescence enhancement as a cytoDATL monomer labeled with Cy3 on an engineered G343C residue in the 3HB (i) undergoes dimerization and crossover (ii). (B and C) PIFE, or fluorescence enhancement (F/Fo), over time for either wild type (B) or R48E (C) Cy3-cytoDATL mixed with the indicated nucleotides. (D) F/Fo over time when wild-type Cy3-cytoDATL is mixed with GTP. (E) F/Fo over time when wild type, R48E, K320E, or the double-mutant variant K320E, E328R is mixed with GMPPNP. For all assays, final concentrations after mixing were 2 µM Cy3-cytoDATL and 1 mM nucleotide. Either a single representative trace (B–D) or the mean of three replicates (±SEM) is shown (E). WT, wild type.

the CFP/YFP sensors, we adapted a method termed protein-induced fluorescence enhancement (PIFE). PIFE, used previously to monitor DNA–protein interactions, takes advantage of the environmental sensitivity of the Cy3 fluorophore (Mujumdar et al., 1993; Gruber et al., 2000). When DNA within 0–4 nm of a protein-binding site is conjugated with Cy3, nearby protein binding reduces the torsional mobility of the Cy3, resulting in distance-dependent fluorescence enhancement (Hwang et al., 2011). When conjugated to G343C of cytoDATL, Cy3 underwent an ∼20% fluorescence enhancement under conditions leading to crossover, as schematized (Fig. 1 A).

As PIFE had not been used previously to monitor crossover, it was important to validate that it works as expected based on previous data. A robust fluorescence enhancement was seen after mixing Cy3-cytoDATL with the nonhydrolyzable GTP analogue GMPPNP, but not GDP or buffer (Fig. 1 B). The time to maximal enhancement ($t_{1/2}$ ∼50 s) was nearly identical to that previously observed for cyto-hATL1-CFP/YFP by FRET (Byrnes et al., 2013). When R48E, a mutation that abrogates nucleotide binding (Bian et al., 2011; Byrnes and Sondermann, 2011), was tested under the same conditions, no enhanced signal was observed with any nucleotide (Fig. 1 C), indicating that crossover, as reflected in the PIFE signal, was induced specifically by GMPPNP binding. Furthermore, as observed previously for cyto-hATL1 CFP/YFP (Byrnes et al., 2013), GTP gave a profound 100-fold acceleration of crossover over that seen with GMPPNP (Fig. 1 D). Thus, PIFE recapitulated key aspects of atlastin crossover and corroborated an earlier study that GTP binding, and hydrolysis in particular, catalyzes atlastin crossover (Byrnes et al., 2013).

Previous work in our laboratory identified two charged residues important for crossover: K320 and E328 (Morin-Leisk et al., 2011; Saini et al., 2014). These residues, conserved between DATL and human atlastins, are at the heart of the crossover dimer and participate in an intramolecular salt bridge in the postfusion conformation. We previously showed that the reversal of charge at either residue in cytoDATL (K320E or E328R) disrupts both crossover and fusion without diminishing steady-state GTPase activity (Morin-Leisk et al., 2011; Saini et al., 2014). Interestingly, the compensatory double-charge reversal mutation (K320E, E328R), predicted to restore charge attraction, appeared to fully restore crossover according to cross-linking assays (Morin-Leisk et al., 2011; Saini et al., 2014), yet it only partially restored fusion activity (Saini et al., 2014). To test if PIFE might offer a more sensitive test for crossover and reveal a mild defect still present in the double-mutant variant, we compared GMPPNP-induced PIFE in wild-type, single-mutant (K320E), and double-mutant (K320E, E328R) variants (Fig. 1 E). As anticipated, the single-mutant variant was strongly impaired, whereas crossover was largely restored in the double-mutant variant. However, a modest defect in crossover, not previously seen with cross-linking, was still observed in the double-mutant variant, with the PIFE signal not yet reaching its maximal value well after the wild-type signal had plateaued (Fig. 1 E). Collectively, these data indicate that PIFE could be a powerful tool for detecting subtle defects in atlastin crossover.

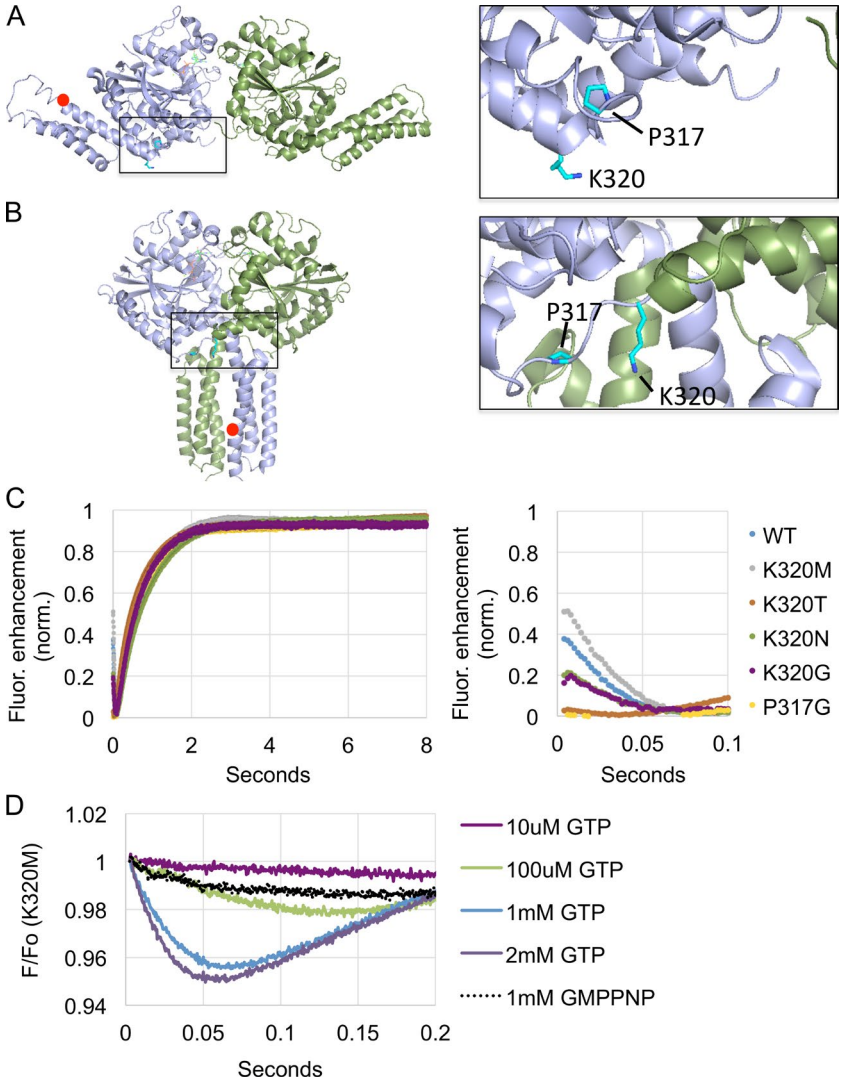

Figure 2. **Mutant variants show no defects in GTP-catalyzed crossover formation.** (A and B, left) The positions of K320 and P317 mutations made to target DATL crossover superimposed onto PyMOL renderings of (A) the hATL1 form2 extended dimer PDB 3QOF and (B) the hATL1 form3 crossover dimer PDB 4IDP. The position of the Cy3 dye in each structure is indicated with a red circle. (A and B, right) Enlargement of the boxed regions in A and B showing the K320 and P317 side chains highlighted in cyan. (C) Normalized PIFE over time when each of the indicated Cy3-cytoDATL mutant variants is mixed with GTP. (C, right) Zoomed-in view of the first 100 ms of the trace in C. The mean of seven runs is shown for each trace (SEM < 0.01) and all traces were repeated with independent protein preps with similar results. (D) A single representative PIFE trace over time when K320M Cy3-cytoDATL is mixed with the indicated concentrations of GTP or GMPPNP. The final concentrations after mixing were 2 µM Cy3-cytoDATL and 1 mM nucleotide unless indicated otherwise. WT, wild type.

Variable disruption of crossover

We next set out to create a panel of atlastin mutant variants with variable disruptions to the crossover state. In addition to being part of a salt bridge, K320 in the crossover dimer is at the heart of a highly spatially restricted bend in the linker between the GTPase head and the 3HB (Byrnes et al., 2013), making it an ideal focal point for additional mutagenesis (Fig. 2, A and B). Further, K320E shows no loss of steady-state GTPase activity despite being defective in both crossover and fusion (Saini et al., 2014), making it an ideal residue to target the crossover conformation specifically. Finally, though we had shown that the creation of charge repulsion with the nearby E328 rendered the charge reversal of this residue (K320E) incapacitating for fusion (Saini et al., 2014), we found, surprisingly, that the salt bridge, by itself, was nonessential for fusion (see Fig. 7 A). Reasoning that a variety of uncharged amino acid substitutions of this residue may provide a range of defects possibly milder than K320E, K320 was replaced with T, M, G, or N. We also included the previously partially characterized P317G variant (Saini et al., 2014) because of both the proximity of the conserved P317 residue to K320 and its unique position as the pivot point of 3HB rotation during crossover (Fig. 2, A and B). As anticipated based on previous GTPase assays of K320E and P317G (Saini et al., 2014), all variants had steady-state GTPase activity similar to the wild type (Fig. S1).

The mutant variants were first analyzed using PIFE under conditions of accelerated crossover with GTP. To emphasize the relative rates of crossover across different mutant variants, the data were normalized to a value of 1 for maximum fluorescence and a value of 0 for minimum fluorescence. The kinetics of crossover was unaffected by normalization (see Fig. S2, A for kinetics before normalization and B for kinetics after normalization). To our surprise, when GTP was added to initiate crossover, no significant difference in crossover rate was observed between the wild-type and any mutant variant (Fig. 2 C, left). The main difference between variants was the magnitude of an early downward deflection that preceded the fluorescence enhancement because of crossover (Fig. 2 C, right). For any given mutant variant, the slope of the downward deflection depended strongly on nucleotide concentration (Fig. 2 D), indicating nucleotide binding as its cause. Based on the proximity of the Cy3-labeled 3HB residue to the GTPase head in the form 2 structure (Fig. 2 A), we suspected that this downward deflection could be caused by a starting Cy3 fluorescence enhancement arising from packing interactions between the 3HB and head (Byrnes et al., 2013), which is subsequently lost as the position of the 3HB is altered upon nucleotide binding. Based on this reasoning, the differences in the magnitude of downward deflection across mutant variants could be attributed to slight

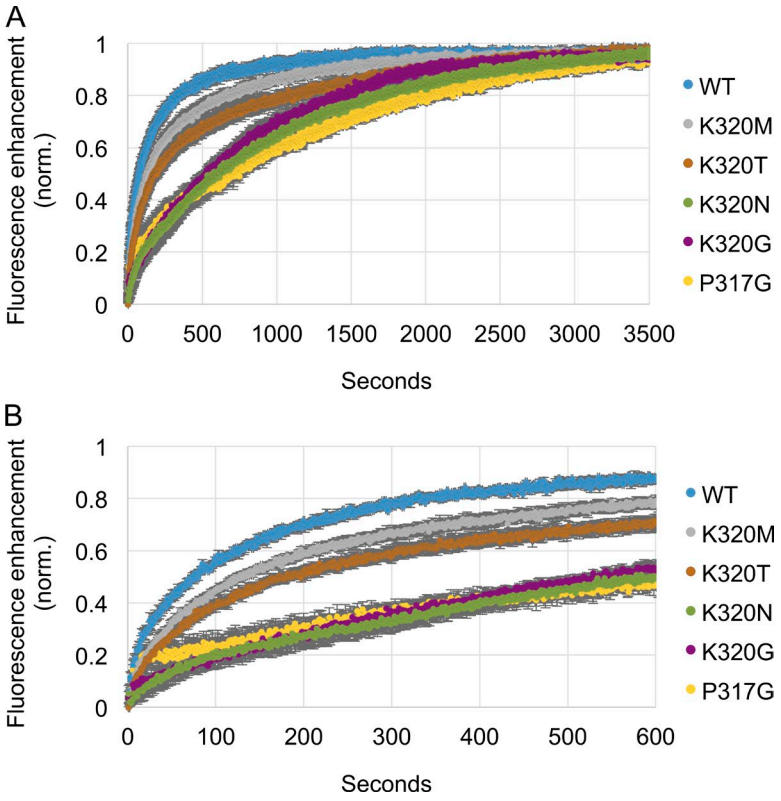

Figure 3. **Mutant variants show defects in GMPPNP-induced crossover.** (A) Normalized PIFE (n = 3 replicates, ±SEM) over time when each of the indicated Cy3-cytoDATL variants is mixed with GMPPNP. (B) Zoomed-in view of the first 600 s of the trace in A. Final concentrations after mixing were 1 µM Cy3-cytoDATL and 1 mM nucleotide. All traces were repeated with independent protein preparations with similar results. WT, wild type.

differences in the extent to which the 3HB is initially packed against the head before nucleotide loading.

The lack of any differences in crossover rates for any of the variants (Fig. 2 C) implied that none were defective in crossover formation. This was surprising, and we wondered whether defects might be better revealed with GMPPNP, which induces crossover 100-fold more slowly than GTP and showed clear differences between various salt bridge mutant variants (Fig. 1 E). When GMPPNP was used to initiate the reaction, crossover defects were readily apparent for K320N, K320G, and P317G (Fig. 3, A and B). In contrast, K320M and K320T showed only a slight or modest defect, respectively. We concluded that some, but not all, of the targeted mutant variants had a defect in either forming or maintaining the crossover state. Given that the defect was evident only during the apparent slow approach to equilibrium induced by GMPPNP (Fig. 3, A and B), we suspected that the main defect in these variants might lie less in the formation and more in the maintenance of the crossover conformation.

Cross-linking confirms certain mutant variants accumulate more slowly in the crossover state

To confirm our observations with fluorescence, we returned to our original cross-linking assay in which we had shown the homo-bi-functional thiol reactive cross-linker bismaleimidoethane (BMOE) to conjugate two 3HB G343C residues to one another exclusively in the crossover state (Saini et al., 2014). To increase the time resolution of the assay, the time of incubation with cross-linker was drastically shortened, from 30 min to 20 s. Additionally, we took advantage of the availability of cysteine reactive cross-linkers of longer lengths to probe for the possibility of more loosely crossed-over conformations, if present. After incubating each variant for either 60 s or 60 min in the presence of GMPPNP, either BMOE, with an 8 Å spacer arm, or methanethiosulfonate (MTS17), with a 24 Å spacer arm (Loo and Clarke, 2001), was used to capture dimers (Fig. 4, A and B). Paralleling results with the PIFE assay with GMP PNP (Fig. 3, A and B), K320N, K320G, and P317G variants were slower to accumulate crossover dimers as compared with wild type, K320M, and K320T. Little or no early products were seen for the former, whereas for the latter, cross-linked products were observed as early as 60 s. Similar results were obtained with both short (Fig. 4 A) and long (Fig. 4 B) cross-linkers, indicating the absence of another discrete, loosely crossed over intermediate en route to full crossover. Finally, confirming previous cross-linking data (Saini et al., 2014) and the PIFE data (Fig. 1 E), the charge reversal variant K320E showed only residual accumulation of crossover dimers with GMPPNP even after 60 min. These data confirmed that the K320N, K320G, and P317G variants had a defect in either forming and/or maintaining the crossover state.

The crossover conformation is destabilized in certain mutant variants

We next tested whether K320N, K320G, and P317G might have a defect in crossover dimer maintenance that could account for the slowed approach to equilibrium seen with GMP PNP (Fig. 3 A). To assess crossover dimer stability, we used FRET to monitor dimer dissociation rates. FRET between Alexa Fluor 488 and Alexa Fluor 647 on an engineered cysteine on the head of each monomer has been used previously to report on cyto-hATL1 head-to-head dimerization kinetics (Byrnes et al., 2013), and we adapted the assay here by targeting the equivalent cysteine residue (S270C) in cytoDATL. Alexa Fluor 488– and Alexa Fluor 647–labeled cytoDATL crossover dimers were first preformed with GMPPNP (Fig. 5 A). The use of the nonhydrolyzable analogue here was necessary to prevent rapid dimer disassembly, which is likely coupled to product

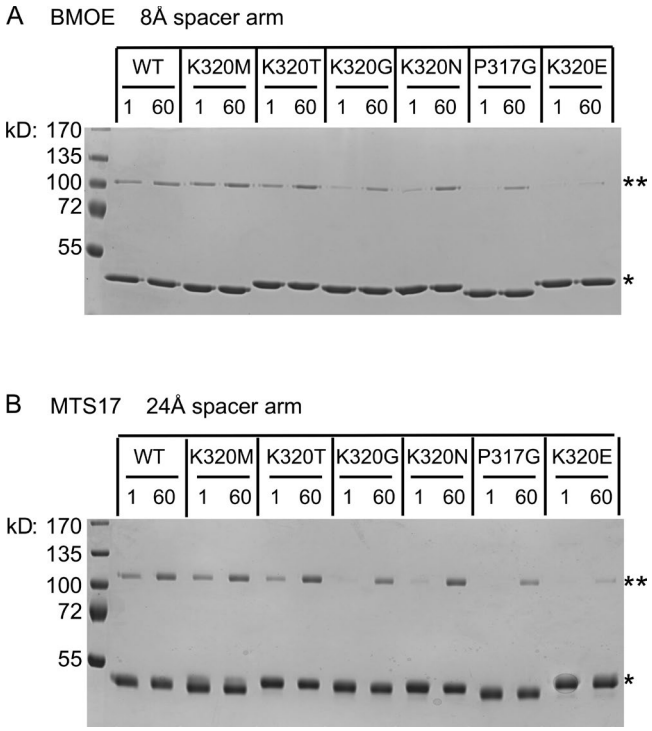

Figure 4. **Cross-linking confirms crossover defects for a subset of mutant variants.** Each of the indicated cytoDATL variants was incubated at RT for either 1 min or 60 min in the presence of GMPPNP and then subjected to 20 s of cross-linking with either BMOE (8 Å spacer arm; A) or MTS17 (24 Å spacer arm; B). The structure of each cross-linker is shown to the right. Cross-linked dimers were resolved by SDS-PAGE and visualized with Coomassie blue. The single asterisk marks the monomer, and the double asterisk marks the cross-linked dimer. All variants had the G343C substitution. Concentrations before cross-linker addition were 2 µM CytoDATL and 1 mM nucleotide. The data shown are representative of at least two independent experiments. WT, wild type.

release after GTP hydrolysis (Byrnes and Sondermann, 2011; Morin-Leisk et al., 2011; Moss et al., 2011). A 60-min initial incubation period with GMPPNP was of sufficient length to ensure that all variants, even those slow to reach equilibrium, had attained their maximal extent of crossover as indicated by a plateau in both FRET and PIFE signals (see Fig. 8 and Fig. 3, respectively). This was followed by addition of excess unlabeled cytoDATL, which should produce a loss of FRET over time as labeled subunits that dissociate will reform new dimers primarily with unlabeled subunits (Fig. 5 A). There was little or no loss of acceptor fluorescence when wild-type crossover dimers were spiked with excess unlabeled wild-type cytoDATL (Fig. 5 B) over that seen when spiked with buffer (Fig. 5 C), indicating that wild-type crossover dimers formed with GMP PNP are stable over the course of 2 h. This essential irreversibility contrasted with the relatively rapid turnover seen previously using the alternate nonhydrolyzable analogue GTPγS (Liu et al., 2015), which may possibly be explained by some hydrolysis of the GTPγS. In contrast to the wild type, K320N, K320G, and P317G, the same variants slow to accumulate in the crossover state with GMPPNP (Figs. 3 and 4), showed accelerated disassembly over the course of 2 h, indicating a loss of crossover dimer stability (Fig. 5 B). Dimerization was still favored for these variants, as indicated by the minimal loss of the FRET signal after buffer addition (Fig. 5 C). In contrast, K320M and K320T were either indistinguishable from the wild type or only slightly destabilized, respectively (Fig. 5 B). We concluded that the targeted mutant variants were variably diminished in crossover dimer stability, with wild type ≈ K320M > K320T >> K320N > P317G > K320G. Moreover, the loss of crossover dimer stability for K320N, K320G, and P317G could account for the slowed accumulation of GMPPNP crossover dimers observed for these variants (Fig. 3) as well as the lower extent of accumulation of crossover dimers for some of the variants even after 1 h (Fig. 4). Unlike the wild-type crossover dimer, which formed essentially irreversibly, the mutant variant crossover dimers underwent significant dissociation, yielding a slowed approach to an equilibrium state of continued crossover formation and loss.

Crossover dimer stability closely parallels fusion activity

To assess the impact of reduced crossover dimer stability on atlastin function, we next looked at the fusion activity of these mutant variants. First, we assessed ER network integrity in cells expressing each mutant variant as a proxy for in vivo fusion functionality (Saini et al., 2014). Typically, overexpression of any fusion incompetent atlastin results in a dominant negative disruption of the ER network and loss of network branching in some fraction of cells, whereas overexpression of a fusion active atlastin causes little or no perturbation (Saini et al., 2014). Wild-type and mutant versions of full-length Venus-DATL were transfected into COS-7 cells, and the fraction of overexpressing cells with a normal branched ER network morphology was visualized (Fig. 6 A) and quantified for each mutant variant (Fig. 6 B). K320M cells were indistinguishable from the wild type, a very small fraction of K320T cells showed ER defects, and ∼50% of K320N cells showed substantial ER disruption. Meanwhile, virtually all K320G and P317G cells showed a loss of normal ER (Fig. S3 shows the full range of abnormal ER morphologies observed for these variants). Based on our prior work (Saini et al., 2014), the results predicted full fusion competence for K320M, slightly reduced fusion for K320T, only residual fusion for K320N, and absence of fusion activity altogether for K320G and P317G.

Fusion activity was directly assessed using a previously described in vitro lipid-mixing assay (Moss et al., 2011; Liu et al., 2015). The full-length version of each DATL variant was inserted at a 1:1,000 protein/lipid ratio into either unlabeled lipid vesicles or vesicles with lipids containing the fluorophores Marina blue (MB) and nitrobenzoxadiazole (NBD), with NBD acting to quench the MB. In the presence of GTP, mixing of labeled and unlabeled vesicles due to either full or hemi-fusion, leads to a de-quenching of the MB. The in vitro lipid mixing activity mirrored the in vivo results (Fig. 7 A). K320M had activity similar to the wild type, whereas K320T had a modest slowing. K320N was capable of some lipid mixing, but at severely reduced levels. Finally, K320G and P317G had undetectable activity. All variants were incorporated into vesicles with similar efficiency (Fig. S4). Overall, in vitro lipid mixing activity correlated remarkably well with crossover dimer stability. To convey the relationship between crossover dimer stability and fusion activity, the apparent dimer dissociation rate for each variant (Fig. 5 B), obtained by a fit to an exponential decay equation (Materials and methods), was plotted against its in vitro lipid mixing activity (Fig. 7 B). The plot underscored the striking correspondence between crossover dimer stability and fusion activity.

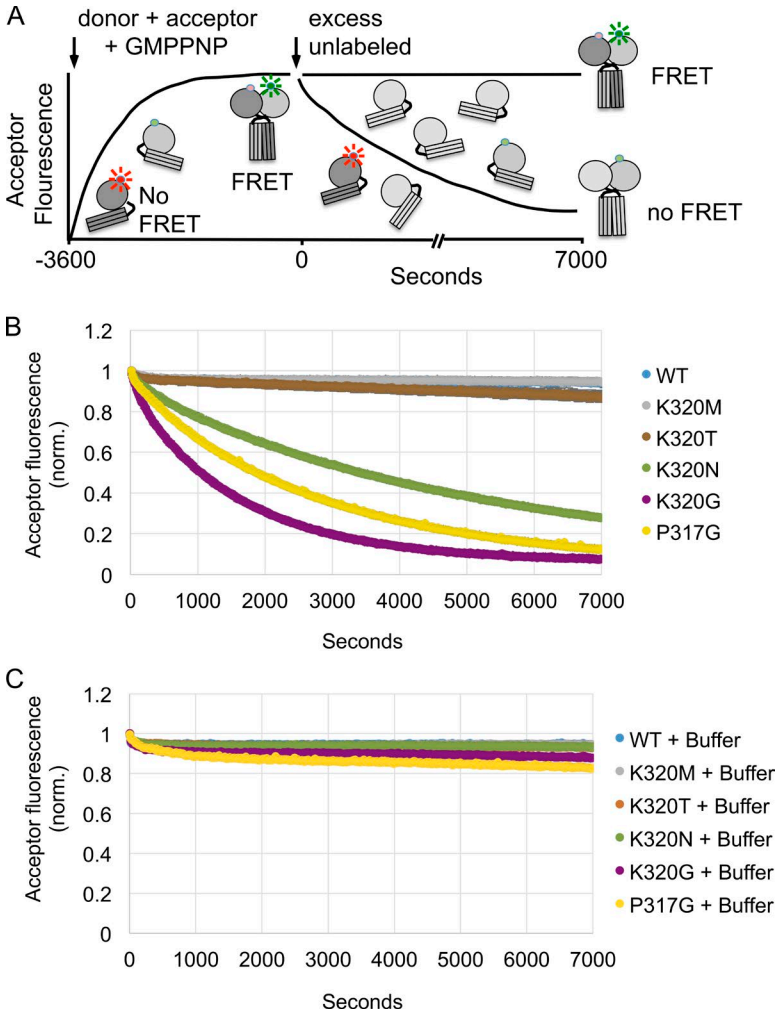

Figure 5. **A subset of mutant variants has decreased crossover dimer stability.** (A) Schematic of the assay. 2 µM of the indicated cytoDATL variants labeled with Alexa Fluor 488/647 at a 1:1 donor/acceptor ratio were incubated with 1 mM GMPPNP (final concentrations) for 60 min to form crossover dimers. After confirming that the FRET-induced acceptor fluorescence signal had plateaued, a fivefold molar excess of the corresponding unlabeled cytoDATL mutant variant was added and the subsequent decay in acceptor signal monitored over time. (B and C) Loss of acceptor fluorescence (n = 3 replicates, ±SEM) after addition of either the corresponding unlabeled competitor protein (B) or buffer (C). WT, wild type.

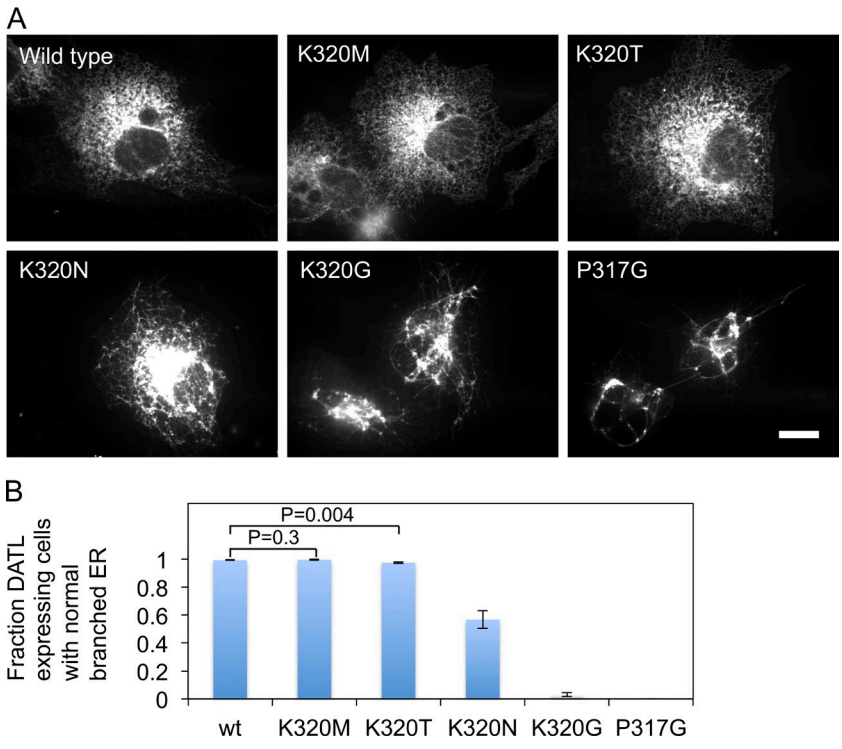

Figure 6. **A subset of mutant variants causes abnormal ER network structure.** (A) COS-7 cells transfected with each indicated variant of full-length Venus-tagged DATL were fixed and imaged 48 h later by confocal microscopy. Bar, 10 µm. (B) Quantification of the percentage of expressing cells displaying a normal branched ER (>100 cells per measurement; data represent mean of three independent measurements ± SD); *, P < 0.0001 (Student's t test) with respect to wild type (wt).

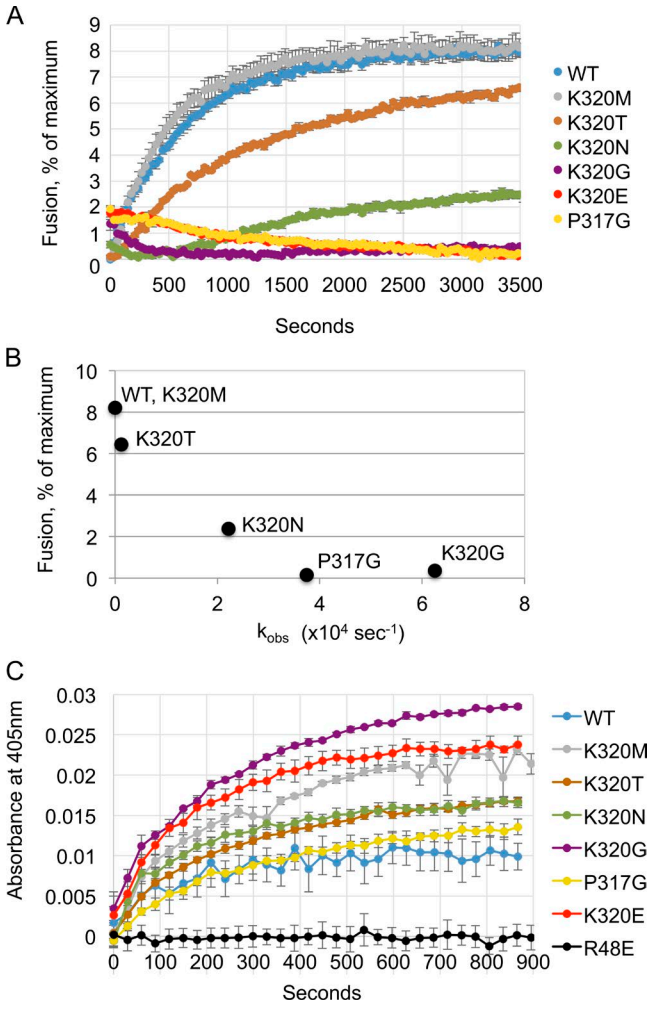

Figure 7. **Crossover dimer stability correlates more closely with fusion than tethering.** (A) Mutant variants are variably defective in in vitro fusion activity. The full-length DATL version of each mutant variant was reconstituted into donor and acceptor vesicles at a 1:1,000 protein/lipid ratio. Fusion was monitored as the dequenching of MB-labeled lipid present in the donor vesicles (0.6 mM total lipid) over time after addition of 1 mM GTP (n = 3 replicates; ±SEM). (B) Fusion activity closely parallels crossover dimer stability. The apparent dissociation rate constant for each variant, calculated by fitting the mean of three traces (from Fig. 5 B) to an exponential decay equation (Materials and methods), is plotted against the mean percent fusion (SEM < 0.3%) in vitro (endpoint of A) achieved by the same variant. (C) Vesicle tethering activity does not correlate with crossover dimer stability. The full-length DATL version of each mutant variant was reconstituted into vesicles at a 1:1,000 protein/lipid ratio (0.6 mM total lipid). Tethering by each variant was monitored as the increase in 405-nm absorbance over time after addition of 1 mM GTP (n = 3 replicates; ±SEM). WT, wild type.

Tethering activity is less dependent on crossover dimer stability

The aforementioned results suggested that the binding energy of the crossover conformation is a key determinant of fusion capacity. However, it did not provide any information on potential impacts on membrane apposition, or tethering. To identify possible kinetic defects in tethering, we turned to a previously established assay based on an increase in light absorbance over time as vesicle tethering produces larger objects that scatter more light, thereby leading to an apparent increase in absorbance (Liu et al., 2015). A full-length version of each DATL mutant variant was inserted into lipid vesicles and the absorbance at 405 nm monitored after GTP addition (Fig. 7 C). As expected (Saini et al., 2014), the nucleotide-binding–defective variant, R48E, showed no tethering activity whatsoever. Also as expected, the wild-type, K320M, and K320T variants all showed robust tethering, with the magnitude of absorbance changes similar to previously reported values for the wild type (Liu et al., 2015). Although not shown here, the majority of the absorbance increase for these fusion active variants was expected to be caused by vesicle tethering, with a minor fraction of the signal arising from increased vesicle size after fusion (Liu et al., 2015). Importantly, for the K320N, K320G, and P317G variants, in which little or no signal was expected from fusion, the absorbance increased well above background levels and at a pace at least as robust as the wild type. The meaning of the differences in amplitude observed with different mutant variants was unclear, as the differences did not correlate with any other parameter; tethering activity and crossover dimer stability appeared to be inversely correlated for certain mutant variant pairs but not for others. Although these data did not rule out a contribution of the crossover binding energy toward tethering, they favored a model in which the energy required for fusion far exceeds that required for tethering, and crossover contributes a more important driving force for fusion.

Hydrolysis catalyzes simultaneous dimerization and crossover

Having established a major role for the crossover dimer conformation for fusion catalysis, we next set out to unravel the sequence of events surrounding crossover formation. Previous work on wild-type hATL1 showed head-to-head dimerization occurring concurrently with crossover, suggesting that the two reactions are catalyzed simultaneously (Byrnes et al., 2013). Speculating that the destabilization of the crossover state in some of the variants might allow for the separation of dimerization and crossover as two rapid, but separable steps, we examined the GMPPNP-induced kinetics of head-to-head dimerization for each mutant variant using the FRET Alexa Fluor 488 and Alexa Fluor 647 donor–acceptor pair of cytoDATL described in Fig. 5. Consistent with the previous study (Byrnes et al., 2013), the kinetics of FRET were similar to the kinetics of PIFE for the wild type (Fig. 8 A), as well as for K320M and K320T (Fig. 8, B and C). However, for K320N, K320G, and P317G (Fig. 8, D–F), the PIFE signal lagged substantially behind the FRET signal. This slowing of crossover relative to head-to-head dimerization for K320N, K320G, and P317G could have resulted from an uncoupling between head-to-head dimerization and crossover formation. Alternatively, it might have resulted from differences in the turnover of head-to-head and/or crossover dimer complexes during the slowed approach to equilibrium with GMPPNP that are not present with GTP.

To distinguish between these alternatives, we examined the kinetics when dimerization was initiated with GTP. Also, to minimize any potential issues in comparing PIFE with FRET kinetics, we replaced the PIFE probe with cytoDATL-mCerulean/SYFP FRET probes for crossover. When the reaction was initiated with GTP, the wild-type kinetics of crossover as monitored by FRET was nearly identical to that seen with PIFE (Fig. 9 A); however, as expected, the downward deflection in the PIFE signal caused by nucleotide binding (Fig. 2 C) was absent in the FRET signal. Consistent with the previous study (Byrnes et al., 2013), the rate of head-to-head dimerization as monitored by FRET was nearly the same

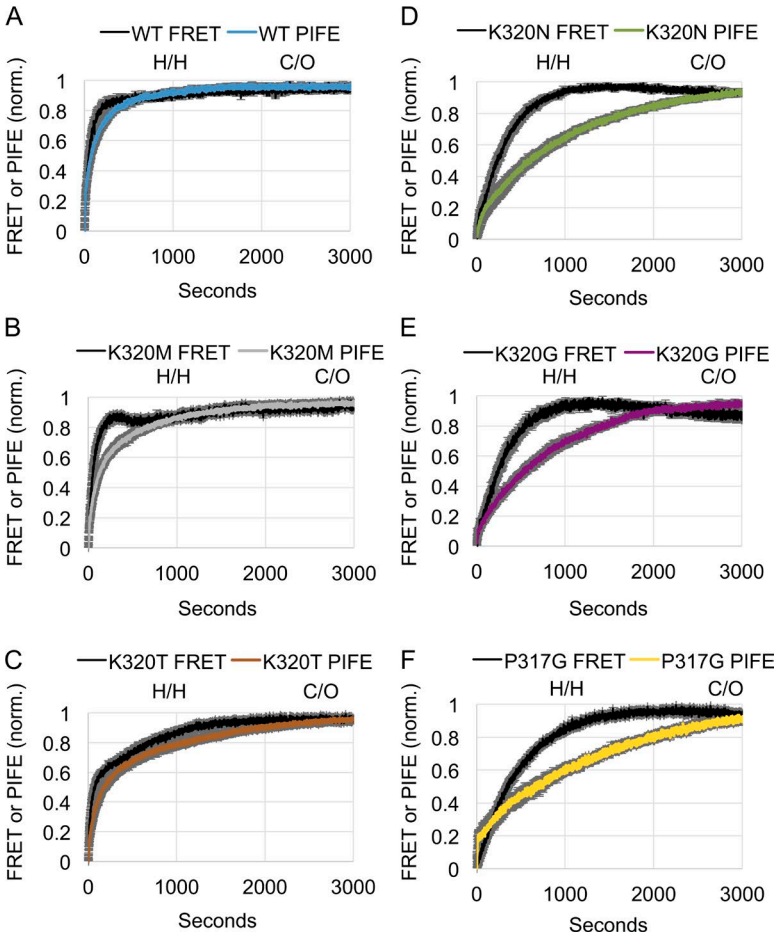

Figure 8. **Head-to-head dimerization occurs before crossover when initiated with GMPPNP.** Measurements of head-to-head dimerization monitored by FRET between wild type (A), K320M (B), K320T (C), K320N (D), K320G (E), and P317G (F) cytoDATL variants. Normalized FRET efficiency (E) = 1 – (I_{DA}/I_D), over time, from mixing 1 µM of the indicated variants with 1 mM GMPPNP, is shown relative to the normalized PIFE traces for each variant obtained in Fig. 3 A using the same concentrations of protein and nucleotide. The mean of three replicates (±SEM) is shown, and the entire set of traces was repeated with independent protein preparations with similar results. WT, wild type.

as crossover FRET (Fig. 9 A); the slight difference was not statistically significant. Under these conditions, K320G, the most severely destabilized variant in the crossover state (Fig. 5 B), also showed concurrent head-to-head dimerization and crossover (Fig. 9 B). Furthermore, there was little or no difference between wild-type and K320G in the initial rate of either head-to-head dimerization (Fig. 9 C) or crossover formation (Fig. 9 D). The fact that no difference could be discerned between wild-type and K320G indicated that dimerization and crossover were inseparable, even in the most severely defective variant, further corroborating a model in which dimerization and crossover occur simultaneously. In addition, the data underscored the highly selective nature of the K320G mutation in its ability to destabilize the crossover conformation without affecting any of the steps leading up to its formation.

Atlastin's GTPase cycle depends on dimerization

The apparent simultaneity of head-to-head dimerization and crossover formation seemed counterintuitive because it implied that unpaired atlastins from opposing membranes might enter into a trans crossover dimer configuration in a single step. However, an alternative interpretation was that atlastins first encounter one another in the GTP-bound state, whereupon hydrolysis is rapidly triggered to catalyze crossover dimer formation. If the initial interaction between GTP-bound heads were the rate-limiting step in the reaction cycle and subsequent steps ensue rapidly, then head-to-head dimerization and crossover formation would appear synchronous as observed (Fig. 9, A and B). Dimerization-dependent hydrolysis of GTP has not been previously reported for atlastins. However, it has been established for human guanylate-binding protein 1 (hGBP1), whose GTPase domain is more similar to atlastin than to any other dynamin-related protein (Zhao et al., 2001). Upon dimerization, the R48 residue in the P-loop of hGBP1, initially facing the dimer interface, swings into the nucleotide-binding pocket to stabilize the transition state (Ghosh et al., 2006). The same residue in atlastin (R77 in hATL1 and R48 in DATL) also faces out toward the dimer interface in the form 2 prefusion structure but is oriented in toward the bound nucleotide in the form 3 crossover dimer structure (Bian et al., 2011). Therefore it was tempting to speculate that dimerization dependent hydrolysis would have been conserved between these two closely related GTPases. To test for this possibility, we monitored the release of GDP at steady state as a measure of the GTPase activity of atlastin in a continuous coupled assay under saturating GTP concentrations but varying atlastin protein concentrations. Notably, as the concentration of cytoDATL fell below those typically used in GTPase assays of atlastin, the observed rate of product release fell accordingly (Fig. 9 E), with a fit of the rates to a simple dimerization equation yielding an estimated dissociation constant of ~0.45 µM. Although additional assays would be required to demonstrate the existence of a GTP-bound trans-dimer, the apparent dependence of the hydrolysis cycle on dimerization was consistent with the possibility.

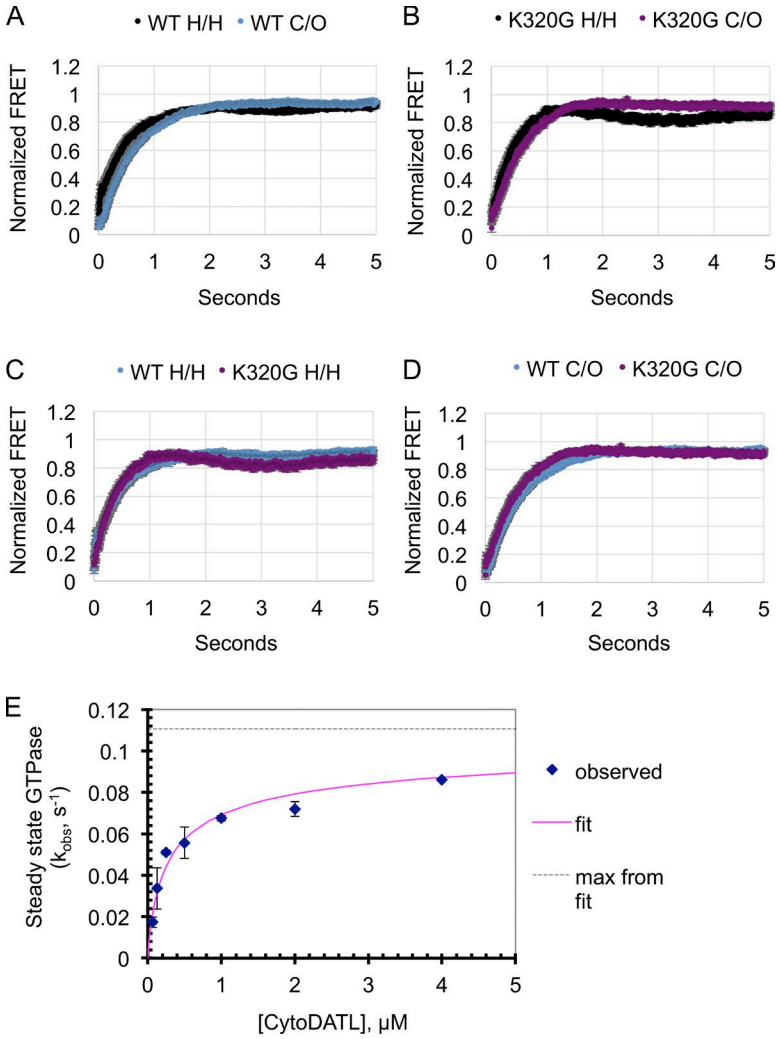

Figure 9. **GTP hydrolysis is concentration dependent and stimulates simultaneous dimerization and crossover.** Relative kinetics of head-to-head dimerization and crossover in wild type (A) and K320G cytoDATL (B) as monitored using FRET. Normalized FRET efficiency (E) = 1 − (I_{DA}/I_D), over time after mixing 1 µM of the appropriate FRET pairs, cytoDATL Alexa Fluor 488/647 for head-to-head dimerization and cytoDATL-mCer/SYFP for crossover, of the indicated variants with 1 mM GTP. Also shown are comparisons between the wild type and K320G with respect to head-to-head dimerization (C) and crossover (D), respectively. The mean of seven replicates (±SEM) is shown, and the entire set of traces was repeated with independent protein preparations with similar results. (E) CytoDATL steady-state GTPase activity varies with protein concentration. The observed GTPase activity (micromoles GDP s^{-1} per micromole cytoDATL) at the indicated concentrations of cytoDATL (n = 3 replicates; ±SD) are plotted and fit to a simple dimerization equation. The data shown are representative of two independent experiments. WT, wild type.

Discussion

Our results are summarized in a working model, essentially a hybrid of earlier models. The model starts with atlastins on opposing membranes (Fig. 10 A) encountering one another in a GTP-bound prefusion conformation (Fig. 10 B), whereupon yet-to-be verified trans interactions between GTP-bound heads induce the rapid reorientation of catalytic residues necessary for GTP hydrolysis, which in turn triggers, in one step, the release of the 3HBs from the heads, strengthening of the head-to-head binding interface and 3HB crossover, to form the postfusion conformation (Fig. 10 C). In the case of wild-type or K320M atlastin, the free energy released through crossover formation, together with the membrane-destabilizing effects of the TM domains and tail, is sufficient to simultaneously draw the membranes into close apposition and to initiate bilayer mixing for fusion (Fig. 10 C). In contrast, in the case of K320N, K320G, or P317G, the binding energy of the crossover conformation is either largely insufficient, or insufficient altogether, to initiate bilayer mixing, leading to a state in which fusion has failed but the membranes remain tethered to one another (Fig. 10 C′). The first step of the model is largely based on the dimerization dependent hydrolysis of GTP observed for hGBP1 (Ghosh et al., 2006), and though consistent with our observations, further experimentation is required to confirm this. Other aspects of the model are supported by the following observations: (a) head-to-head dimerization and crossover formation occur concurrently, (b) mutant variants with a destabilized crossover conformation can generate a tethered state but are incapable of progressing to fusion, and (c) the binding energy of the crossover conformation closely parallels fusion capacity.

Even with its distinct architecture and enzymatic properties, a strong analogy can be drawn between atlastin and previously studied fusion protein catalysts, where a major driving force for membrane fusion comes from a set of highly favorable protein–protein interactions that convert the catalyst from a prefusion to postfusion state. The amount of energy released per atlastin crossover dimer, and how it compares to that of viral fusion protein and SNARE postfusion complexes, remains to be determined. For the SNAREs, the binding energy of the postfusion complex has been measured to be 30–40 k_BT (Yersin et al., 2003; Liu et al., 2006; Li et al., 2007; Gao et al., 2012), remarkably similar to the theoretical 40–50 k_BT estimated energy barriers for fusion (Cohen and Melikyan, 2004); however, because of the quasi-irreversibility of the postfusion states of both SNAREs and viral fusion proteins (Carr et al., 1997; Fasshauer et al., 2002), unconventional approaches have been required. The atlastin crossover dimer seems at least qualitatively similar, with no apparent dissociation over the course of 2 h. It will be of interest in future studies to apply to atlastin the kinds of approaches used for the other fusion proteins.

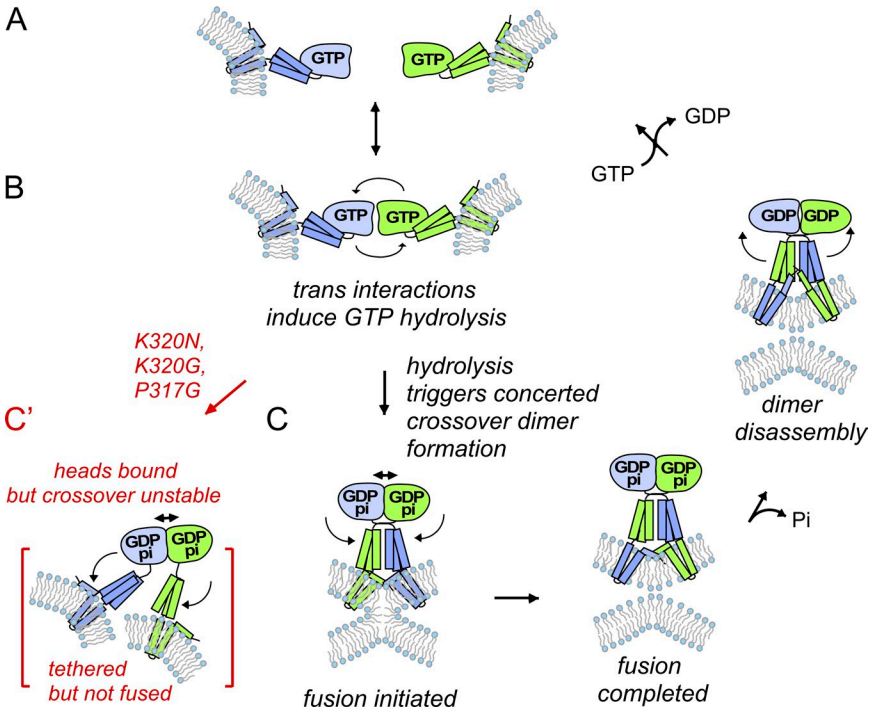

Figure 10. **Working model for atlastin-catalyzed membrane fusion.** GTP-bound atlastins on opposing membranes (A) encounter one another (B). This induces GTP hydrolysis, which triggers simultaneous tightening of the head-to-head interface and formation of the crossover dimer to initiate membrane fusion (C). When the crossover conformation is destabilized by the indicated mutations, fusion fails, resulting in a tethered state (C′).

It should be noted that our working model stems from the results of assays both in the soluble phase and those in the context of membranes. Tethering and fusion reactions are performed, by definition, using the full-length protein anchored in vesicle membranes. However, preparing the full-length protein in vesicles appropriately labeled for the same kinds of assays that have been performed in the soluble phase remains a challenge. Therefore, the kinetic behavior of atlastin in the context of membranes is extrapolated from that in the soluble phase, and the full effects of the added load of the lipid bilayer will need to be assessed in future work. For instance, the extent to which membrane-anchored atlastin achieves the tight crossover conformation seen in the form 3 crystal structure as it undergoes fusion catalysis remains to be seen. Moreover, crossover formation in the soluble phase remained favorable even in the face of mutations that were destabilizing to the crossover state; however, the effects of membrane load on the favorability of crossover formation remain unknown. Presumably, crossover formation will be much less favored when coupled to the work of membrane fusion catalysis.

Finally, although this study has focused on the role of crossover in fusion, it cannot be overstated that fusion catalysis requires more. As noted, membrane insertion of an amphipathic helix in the C-terminal tail of atlastin is also required (Liu et al., 2012; Faust et al., 2015), as are specific residues in the TM domain. As crossover formation, the tail, or the precise sequence of the TM domain is not required to reach the tethered state (Saini et al., 2014; Liu et al., 2015) but all are required for fusion (Liu et al., 2012; Saini et al., 2014; Faust et al., 2015), it may be that all of these mechanisms work in close conjunction and collectively to reduce the energy barrier to lipid mixing. In the absence of any one of these energetic contributions, the activation energy for fusion may be too high, thereby preventing fusion catalysis. Indeed, crossover dimer formation, likely closely coupled to the initiation of bilayer mixing, may fail to occur altogether in the absence of the energetic contributions of either the tail or TM domain. Trans interactions between opposing membrane-spanning domains could provide an additional driving force, though it is currently not known whether the trans interactions of the atlastin crossover dimer extend into the TM region as proposed for previously studied postfusion complexes (Tamm, 2003; Stein et al., 2009). Furthermore, as the atlastin fusion mechanism is ultimately driven by GTP hydrolysis, the maximum free energy liberated by a single atlastin dimer during crossover is unlikely to exceed the total energy of hydrolysis of two molecules of GTP and is thus unlikely sufficient on its own to offset the estimated activation energy (40–50 k_BT) for fusion. cis interactions between the membrane spanning domains, previously reported to occur independently of GTP (Liu et al., 2012), may help coordinate the activity of multiple atlastin dimers. A full understanding of the atlastin fusion mechanism will require the identification of all these additional binding interactions and their relative energetic contributions.

Materials and methods

Cells, constructs, and reagents

Cell expression studies were in COS-7 cells maintained at 37°C in a 5% CO_2 incubator in DMEM (Sigma-Aldrich) with 10% fetal bovine serum (Atlanta Biologicals) and 1% penicillin/streptomycin (Thermo Fisher Scientific). The following constructs were considered wild type for their respective assays, with further mutations created using QuikChange mutagenesis (QIAGEN) and confirmed through sequencing of the full construct (GENEWIZ). All PIFE, cross-linking, and GTPase assays used a previously described (Saini et al., 2014) 6xHis-tagged *D. melanogaster* atlastin (DATL) soluble domain construct (aa 1–415) cloned into the pRSETB vector at NheI and EcoRI sites and containing an engineered cysteine at G343C in the 3HB. FRET assays for head-to-head dimerization used the same construct as for PIFE except that it lacked the G343C mutation and instead had an engineered cysteine S270C based on an equivalent mutation previously described in hATL1 (Byrnes et al., 2013). FRET assays for crossover used the same construct as for PIFE but lacking the G343C mutation and with either

mCerulean3 (mCer3) or super YFP at the C terminus. These were generated by QuikChange insertion of a linker sequence encoding the amino acids GTSTSGHG after AA415 of DATL followed by an NcoI site, into which the PCR-amplified coding sequence of mCer3 or super YFP (AA2-end) was inserted. Cell expression studies used a previously described N-terminally tagged Venus-DATL construct (Saini et al., 2014; Faust et al., 2015). Fusion and tethering assays used a previously described 6xHis-tagged full-length DATL construct in a background of the mutations G343C, C429L, C452L, C501A, and C350A, where the parent construct was generated by cloning a pcr-amplified fragment coding for DATL aa 1–541 into the NheI and EcoRI sites in pRSE TB. This cysteine-substituted construct has fusion activity similar to the parent wild type (Saini et al., 2014). All lipids were purchased from Avanti Polar Lipids, Inc. Nucleotides were purchased from Sigma-Aldrich, reconstituted to 100 mM stocks in 10 mM Tris, 1 mM EDTA, pH 8.0, and stored at −80°C. GTP for the GTPase assay was an exception, reconstituted to 40 mM in 50 mM Tris, 40 mM $MgCl_2$, pH 8.0, adjusted to pH 7. BMOE was purchased from Thermo Fisher Scientific, and MTS17 was from Toronto Research Chemicals.

Protein expression and purification

Expression and purification of DATL was performed as previously described (Morin-Leisk et al., 2011; Saini et al., 2014). In short, DATL expression used a pRSETB vector in BL21(DE3)pLysS *Escherichia coli*. Cells were grown at 25°C to OD ∼0.5 and induced with 0.5 mM (for cytoDATL) or 0.2 mM (for full-length DATL) IPTG. After induction, cells were allowed to express atlastin either overnight at 20°C (cytoDATL) or for 2.5 h at 16°C (full-length DATL). Purification of the soluble domain used standard protocols and buffers for the purification of 6xHis-tagged proteins on Ni-NTA agarose (QIAGEN). Purification of the full-length protein used the following modifications of the standard protocol. Cells were lysed in 4% Triton X-100 (Roche) in the standard lysis buffer, all wash buffers contained 0.1% Triton X-100, and elution was in 50 mM Tris, pH 8.0, 250 mM imidazole, 100 mM NaCl, 5 mM $MgCl_2$, 10% glycerol, 2 mM 2-mercaptoethanol, 0.1% Anapoe-X 100 (Affymetrix), and 1 mM EDTA. Peak fractions typically 4–8 mg/ml (∼1 mg per liter culture) were flash frozen in liquid N_2 and stored at −80°C.

Fluorescence microscopy

COS-7 cells grown on 12-mm glass coverslips (24-well plate, 0.5 ml volume per well) were transfected with 100 ng of the indicated Venus-DATL plasmids and 1.5 µl Lipofectamine 2000 transfection reagent (Thermo Fisher Scientific) according to the manufacturer's instructions. Cells were fixed with 3% paraformaldehyde 48 h later, and images were acquired with a spinning-disk confocal scanhead (Yokagawa; PerkinElmer) mounted on an Axiovert 200 microscope (ZEI SS) with a 100× 1.4 NA objective (ZEISS) and acquired using a 12-bit ORCA ER camera (Hamamatsu Photonics). Maximal value projections of sections at 0.2-µm spacing were acquired using Micro-manager open-source software (University of California, San Francisco).

Fluorescent dye Labeling

For PIFE, cytoDATL containing an engineered cysteine at G343C was desalted by centrifuging through a 5-ml column (Thermo Fisher Scientific) containing 4 ml bed volume of Sephadex G-25 (Sigma-Aldrich) preequilibrated with labeling buffer (25 mM Tris, pH 7.0, 100 mM NaCl, 5 mM $MgCl_2$, 2 mM EGTA, 1 mM imidazole, and 500 µM TCEP). Cy3 maleimide (GE Healthcare, Thermo Fisher Scientific) was added at a 1:1 protein/dye molar ratio. The reaction was incubated for 2 h at RT before being spun at 100,000 rpm (TLA100 rotor; Beckman Coulter) for 15 min at 4°C to remove any precipitate. Labeled cytoDATL was then desalted twice through a column preequilibrated with SEC buffer (25 mM Tris, pH 7.0, 100 mM NaCl, 5 mM $MgCl_2$, and 2 mM EGTA) to remove free Cy3. Typical labeling efficiencies were 20–30%. Cy3 labeling for PIFE in Fig. 1 (B, C, and E) proceeded with the following exceptions: a 1:2 protein/dye ratio in SEC buffer was used, and only a single desalting step followed labeling. For head-to-head FRET, labeling with Alexa Fluor 488 C_5 maleimide and Alexa Fluor 647 C_2 maleimide (Thermo Fisher Scientific) proceeded with two desalting steps, except the S270C construct for FRET assays was used in place of the G343C construct, and the incubation time with dye was reduced to 30 min. Typical labeling efficiencies were 50–70%.

PIFE assays

For GMPPNP PIFE kinetics (Fig. 3), cytoDATL labeled with Cy3 was mixed with 1 mM nucleotide (final) using a stopped flow accessory mounted on a PTI QuantaMaster-400 fluorometer (Horiba Instruments Inc.) and 570-nm fluorescence was monitored at 1-s intervals after 540-nm excitation. Data were acquired using the FelixGX software (Horiba Instruments Inc.) and normalized using the following equation: (fluorescence − minimum fluorescence observed)/(maximum fluorescence observed − minimum fluorescence observed). All data shown represent the mean of three runs per mutant variant. PIFE data in Fig. 1 (B, C, and E) were captured using a Tecan M1000 (Tecan Group Ltd.), and either a single representative trace (Fig. 1, B and C) or the mean of three runs (Fig. 1 E) is shown. For GTP kinetics (Fig. 1 D and Fig. 2, C and D), cytoDATL labeled with Cy3 was mixed with GTP in a stopped flow device (Applied Photophysics SX20). Cy3 was excited at 540 nm, and the resulting change in fluorescence emission was observed with a 560-nm long-pass filter at 2.5-ms intervals. Plotted data were the mean of seven runs per mutant variant. Data were normalized and all PIFE data were replicated with similar results from at least two independent protein preps. All PIFE assays were performed at 25°C in SEC buffer with 2 mM β-mercaptoethanol. All data analysis was performed in Microsoft Excel.

FRET assays

Head-to-head dimerization kinetics was monitored by adapting a FRET assay previously described for atlastin 1 (Byrnes et al., 2013). CytoDATL labeled with Alexa Fluor 488 (donor) and Alexa Fluor 647 (acceptor) at a 1:2 donor/acceptor ratio (1 µM total cytoDATL final) was mixed with 1 mM nucleotide (final). GMPPNP kinetics used the stopped flow attachment on the PTI-QuantaMaster400 fluorometer with a second emission monochromator. After mixing with GMPPNP, the donor (in the presence or absence of acceptor) was excited at 490 nm, and both donor and acceptor fluorescence emission was monitored at 1-s intervals at 520 and 670 nm, respectively. Because of lowered instrument noise in the donor channel, FRET efficiency was calculated from the donor signal using the equation: $E = 1 - (I_{DA}/I_D)$, where E is FRET efficiency, I_{DA} is the donor intensity in presence of acceptor, and I_D is donor intensity in absence of acceptor. FRET efficiency across mutant variants was normalized in the same way as the PIFE data, and all traces represent the mean of three runs per mutant variant. GTP kinetics used the stopped flow device (SX20; Applied Photophysics). After mixing with GTP, the donor was excited at 470 nm, and donor fluorescence emission was monitored with a 520/30 bandpass filter at 2.5-ms intervals. As in the above, FRET efficiency was calculated from the donor signal. For GTP kinetics, the data shown represent the mean of at least seven runs per mutant variant. Crossover FRET kinetics with GTP was monitored by adapting a previously described assay for hATL1 (Byrnes et al., 2013). CytoDATL-mCer3 and cytoDATL-SYFP at a 1:2 donor/acceptor ratio was mixed with GTP in the stopped flow device. Donor was excited at 433 nm, and donor fluorescence emission in the presence or absence of acceptor was monitored with a 480/40-nm bandpass filter

at 2.5-ms intervals. At least seven runs were averaged. FRET efficiency was calculated and the data normalized as above. All assays were performed in SEC buffer + 2 mM 2-mercaptoethanol at 25°C. All FRET data were replicated with similar results from at least two independent protein preps. All data analysis was performed in Microsoft Excel.

For measurement of crossover dimer stability, a modified form of a previously described assay was used (Liu et al., 2015). 2 µM total Alexa Fluor 488– and Alexa Fluor 647–labeled DATL (1:1 donor/acceptor) was incubated at 28°C for 10 min in a Tecan Safire 2 plate reader, and a baseline of acceptor fluorescence was taken by excitation of the donor at 490 nm and measuring acceptor emission at 670 nm. After this, 1 mM GMPPNP was added and allowed to incubate for 1 h at 28°C. After confirming a plateau in the FRET signal, a fivefold molar excess of the corresponding unlabeled cytoDATL variant or buffer (50 µl added to a reaction volume of 200 µl) was added to the reaction mixture, and acceptor fluorescence was monitored at 1-s intervals for 2 h. Data were normalized using the following equation: (fluorescence − minimum)/(maximum − minimum), where minimum was the initial baseline and maximum was the starting value just after the unlabeled cytoDATL was added. Each trace is the mean of three experimental replicates. Apparent k values were calculated by fitting the averaged data to a double exponential curve. Of the two components to the fit, the small-amplitude (<0.12) faster ($t_{1/2}$ <60 s) component was present in all mutant variants with kinetics similar to the buffer control and assumed not to reflect the atlastin off rate. The reported k values are for the slower, larger-amplitude component that varied by mutant variant. The k values for wild type and K320M were assumed to be zero, as little or no signal loss was observed over 2 h compared with buffer alone. All assays were performed in SEC buffer with 2 mM 2-mercaptoethanol.

Proteoliposome production and fusion assay

Lipids in chloroform dried down by rotary evaporation were hydrated by resuspension in A100 buffer (25 mM Hepes, pH 7.4, 100 mM KCl, 10% glycerol, 2 mM 2-mercaptoethanol, and 1 mM EDTA containing 5 mM $MgCl_2$) at a final lipid concentration of ∼10 mM and subjected to 12 freeze–thaw cycles in liquid N_2 and RT water. Liposomes (100–300 nm diameter) were formed by extrusion through 100-nm polycarbonate filters using the LipoFast LF-50 extruder (Avestin) and checked for size by dynamic light scattering (Zen3600; Malvern Instruments). Full-length DATL was inserted at a 1:1,000 ratio of proteins to lipids into labeled and unlabeled populations of liposomes at an effective detergent-to-lipid ratio of ∼0.7 by incubating protein and lipid at 4°C for 1 h followed by detergent removal by SM-2 Bio-Beads (Bio-Rad) at 1 g beads per 70 mg Anapoe X-100. Insoluble protein aggregates were pelleted by centrifugation of the samples in a microcentrifuge for 10 min at 16,000*g*. Thereafter, reconstituted proteoliposomes were adjusted to 50% Nycodenz (Axis-Shield) and separated from unincorporated protein by flotation through a (50%/45%/0%) Nycodenz 5-ml step gradient made in A100 buffer without glycerol. After centrifugation at 40,000 rpm for 16 h at 4°C in a SW50.1 rotor (Beckman Coulter), the gradient was fractionated and analyzed by SDS-PAGE to assess insertion efficiency. Finally, the floated fraction was desalted over a 2.4-ml Sephadex A (GE Healthcare) column into A100 buffer and stored at -80°C until use (Moss et al., 2011; Saini et al., 2014). Unlabeled vesicles consisted of 1-palmitoyl-2-oleoyl-sn-glycero-3-phosphocholine and 1,2-dioleoyl-sn-glycero-3-phospho-L-serineat an 85:15 ratio. Labeled vesicles consisted of 1-palmitoyl-2-oleoyl-sn-glycero-3-phosphocholine, 1,2-dioleoyl-sn-glycero-3-phospho-L-serine, MB, and NBD at an 82:15:1.5:1.5 ratio. For the fusion assay, proteoliposomes (0.6 mM total lipid) were incubated in A100 buffer at a 1:2 ratio of labeled/unlabeled proteoliposomes. After a 10-min incubation at 37°C, 2 mM GTP was added to the proteoliposome mixture, and fluorescence dequenching of MB was monitored every 30 s for 1 h by exciting at 370 nm and measuring the emission at 465 nm using a Tecan M1000 plate reader. After this, 0.5% Anapoe X-100 was added to the mixture to disrupt the liposomes for determination of the maximal possible dequenching. Data were plotted using the following equation: (fluorescence − minimum)/(maximum − minimum), and the mean of three runs was graphed.

Tethering assay

Tethering activity was monitored using labeled vesicles with full-length DATL inserted at a 1:1,000 protein/lipid ratio (0.6 mM total lipid) in A100 buffer containing 5 mM $MgCl_2$ as in the fusion assay described in the previous section. After a 10-min incubation at 37°C, 2 mM GTP or an equivalent amount of buffer was added and the absorbance of each reaction was monitored at 405 nm every 30 s for 1 h in a Tecan M1000. For each run, the absorbance of the proteoliposomes without GTP was subtracted from the absorbance with GTP, and the mean of three runs was graphed.

GTPase assay

GTPase activity was measured as previously described (Hackney and Jiang, 2001) using a continuous coupled assay in which the hydrolysis product GDP serves as cosubstrate in a reaction catalyzed by pyruvate kinase: PEP + GDP → pyruvate + GTP. The pyruvate in turn is reduced by lactate dehydrogenase in a reaction coupled to the oxidative loss of NADH (to NAD^+), which is measured as 340 nm absorbance in a spectrophotometer. Each assay contained 2 mM PEP, 0.1 mg/ml pyruvate kinase, 0.15 mM NADH, and 6 µg/ml lactate dehydrogenase in 200 µl SEC buffer. After preincubation at 25°C with the indicated concentrations of cytoDATL, Mg-GTP was added to 1 mM and NADH absorbance at 340 nm monitored over time at 25°C to obtain the reaction rate for three independent measurements, which was subsequently divided by the cytoDATL concentration to obtain k_{obs}. Each data point represents the mean of three replicates.

Cross-linking

The cross-linking assay was as previously described, except modified to greatly shorten the cross-linking time (Saini et al., 2014). 2 µM atlastin was mixed with 1 mM GMPPNP in SEC buffer at RT to initiate the crossover reaction. After an incubation time of either 1 min or 1 h, the reaction mixture was diluted 1:1 with 100 µM cross-linker (50 µM final), either BMOE or MTS17. After 20 s, the reaction was quenched by diluting 1:1 with 50 mM DTT for BMOE or 20 mM *N*-ethylmaleimide for MTS17 (25 mM or 10 mM final, respectively). The cross-linked samples were then resolved by SDS-PAGE to determine the level of cross-linking. The data shown are representative of at least two independent experiments.

Online supplemental material

Fig. S1 shows that all cytoDATL variants have similar steady-state GTPase activity. Fig. S2 shows that normalization does not alter PIFE kinetics. Fig. S3 shows the range of ER morphological changes in response to expression of the most severely destabilized crossover mutant variants K320G and P317G Venus-DATL. Fig. S4 shows a similar extent of incorporation of each DATL mutant variant into proteoliposomes.

Acknowledgments

M. Bruchez and J. Minden (Carnegie Mellon University, Pittsburgh, PA) shared instruments, M. Bruchez gave helpful advice on the fluorescence assays, C. Telmer (Carnegie Mellon University) provided mCer3 and SYFP, S. Saini and A. Linstedt (Carnegie Mellon University) provided helpful comments on the manuscript, and anonymous reviewers made important suggestions that improved the study.

This work was funded by National Institutes of Health grant R01GM107285 (to T.H. Lee) and supplement R01GM107285-02S1.

The authors declare no competing financial interests.

Author contributions: J. Winsor and T.H. Lee designed and carried out the experiments; J. Winsor, D.D. Hackney, and T.H. Lee analyzed the data; and T.H. Lee and J. Winsor wrote the manuscript.

Submitted: 15 September 2016
Revised: 17 January 2017
Accepted: 17 February 2017

References

Bian, X., R.W. Klemm, T.Y. Liu, M. Zhang, S. Sun, X. Sui, X. Liu, T.A. Rapoport, and J. Hu. 2011. Structures of the atlastin GTPase provide insight into homotypic fusion of endoplasmic reticulum membranes. *Proc. Natl. Acad. Sci. USA.* 108:3976–3981. http://dx.doi.org/10.1073/pnas.1101643108

Byrnes, L.J., and H. Sondermann. 2011. Structural basis for the nucleotide-dependent dimerization of the large G protein atlastin-1/SPG3A. *Proc. Natl. Acad. Sci. USA.* 108:2216–2221. http://dx.doi.org/10.1073/pnas.1012792108

Byrnes, L.J., A. Singh, K. Szeto, N.M. Benvin, J.P. O'Donnell, W.R. Zipfel, and H. Sondermann. 2013. Structural basis for conformational switching and GTP loading of the large G protein atlastin. *EMBO J.* 32:369–384. http://dx.doi.org/10.1038/emboj.2012.353

Carr, C.M., C. Chaudhry, and P.S. Kim. 1997. Influenza hemagglutinin is spring-loaded by a metastable native conformation. *Proc. Natl. Acad. Sci. USA.* 94:14306–14313. http://dx.doi.org/10.1073/pnas.94.26.14306

Chen, Y.A., and R.H. Scheller. 2001. SNARE-mediated membrane fusion. *Nat. Rev. Mol. Cell Biol.* 2:98–106. http://dx.doi.org/10.1038/35052017

Cohen, F.S., and G.B. Melikyan. 2004. The energetics of membrane fusion from binding, through hemifusion, pore formation, and pore enlargement. *J. Membr. Biol.* 199:1–14. http://dx.doi.org/10.1007/s00232-004-0669-8

Daumke, O., and G.J. Praefcke. 2011. Structural insights into membrane fusion at the endoplasmic reticulum. *Proc. Natl. Acad. Sci. USA.* 108:2175–2176. http://dx.doi.org/10.1073/pnas.1019194108

Eckert, D.M., and P.S. Kim. 2001. Mechanisms of viral membrane fusion and its inhibition. *Annu. Rev. Biochem.* 70:777–810. http://dx.doi.org/10.1146/annurev.biochem.70.1.777

Fasshauer, D., W. Antonin, V. Subramaniam, and R. Jahn. 2002. SNARE assembly and disassembly exhibit a pronounced hysteresis. *Nat. Struct. Biol.* 9:144–151. http://dx.doi.org/10.1038/nsb750

Faust, J.E., T. Desai, A. Verma, I. Ulengin, T.L. Sun, T.J. Moss, M.A. Betancourt-Solis, H.W. Huang, T. Lee, and J.A. McNew. 2015. The atlastin C-terminal tail is an amphipathic helix that perturbs the bilayer structure during endoplasmic reticulum homotypic fusion. *J. Biol. Chem.* 290:4772–4783. http://dx.doi.org/10.1074/jbc.M114.601823

Frolov, V.A., and J. Zimmerberg. 2010. Cooperative elastic stresses, the hydrophobic effect, and lipid tilt in membrane remodeling. *FEBS Lett.* 584:1824–1829. http://dx.doi.org/10.1016/j.febslet.2010.01.039

Gao, Y., S. Zorman, G. Gundersen, Z. Xi, L. Ma, G. Sirinakis, J.E. Rothman, and Y. Zhang. 2012. Single reconstituted neuronal SNARE complexes zipper in three distinct stages. *Science.* 337:1340–1343. http://dx.doi.org/10.1126/science.1224492

Ghosh, A., G.J. Praefcke, L. Renault, A. Wittinghofer, and C. Herrmann. 2006. How guanylate-binding proteins achieve assembly-stimulated processive cleavage of GTP to GMP. *Nature.* 440:101–104. http://dx.doi.org/10.1038/nature04510

Gruber, H.J., C.D. Hahn, G. Kada, C.K. Riener, G.S. Harms, W. Ahrer, T.G. Dax, and H.G. Knaus. 2000. Anomalous fluorescence enhancement of Cy3 and cy3.5 versus anomalous fluorescence loss of Cy5 and Cy7 upon covalent linking to IgG and noncovalent binding to avidin. *Bioconjug. Chem.* 11:696–704. http://dx.doi.org/10.1021/bc000015m

Hackney, D.D., and W. Jiang. 2001. Assays for kinesin microtubule-stimulated ATPase activity. *Methods Mol. Biol.* 164:65–71.

Hwang, H., H. Kim, and S. Myong. 2011. Protein induced fluorescence enhancement as a single molecule assay with short distance sensitivity. *Proc. Natl. Acad. Sci. USA.* 108:7414–7418. http://dx.doi.org/10.1073/pnas.1017672108

Jahn, R., and R.H. Scheller. 2006. SNAREs--engines for membrane fusion. *Nat. Rev. Mol. Cell Biol.* 7:631–643. http://dx.doi.org/10.1038/nrm2002

Kozlov, M.M., H.T. McMahon, and L.V. Chernomordik. 2010. Protein-driven membrane stresses in fusion and fission. *Trends Biochem. Sci.* 35:699–706. http://dx.doi.org/10.1016/j.tibs.2010.06.003

Kuzmin, P.I., J. Zimmerberg, Y.A. Chizmadzhev, and F.S. Cohen. 2001. A quantitative model for membrane fusion based on low-energy intermediates. *Proc. Natl. Acad. Sci. USA.* 98:7235–7240. http://dx.doi.org/10.1073/pnas.121191898

Li, F., F. Pincet, E. Perez, W.S. Eng, T.J. Melia, J.E. Rothman, and D. Tareste. 2007. Energetics and dynamics of SNAREpin folding across lipid bilayers. *Nat. Struct. Mol. Biol.* 14:890–896. http://dx.doi.org/10.1038/nsmb1310

Liu, T.Y., X. Bian, S. Sun, X. Hu, R.W. Klemm, W.A. Prinz, T.A. Rapoport, and J. Hu. 2012. Lipid interaction of the C terminus and association of the transmembrane segments facilitate atlastin-mediated homotypic endoplasmic reticulum fusion. *Proc. Natl. Acad. Sci. USA.* 109:E2146–E2154. http://dx.doi.org/10.1073/pnas.1208385109

Liu, T.Y., X. Bian, F.B. Romano, T. Shemesh, T.A. Rapoport, and J. Hu. 2015. Cis and trans interactions between atlastin molecules during membrane fusion. *Proc. Natl. Acad. Sci. USA.* 112:E1851–E1860. http://dx.doi.org/10.1073/pnas.1504368112

Liu, W., V. Montana, J. Bai, E.R. Chapman, U. Mohideen, and V. Parpura. 2006. Single molecule mechanical probing of the SNARE protein interactions. *Biophys. J.* 91:744–758. http://dx.doi.org/10.1529/biophysj.105.073312

Loo, T.W., and D.M. Clarke. 2001. Determining the dimensions of the drug-binding domain of human P-glycoprotein using thiol cross-linking compounds as molecular rulers. *J. Biol. Chem.* 276:36877–36880. http://dx.doi.org/10.1074/jbc.C100467200

Markin, V.S., and J.P. Albanesi. 2002. Membrane fusion: Stalk model revisited. *Biophys. J.* 82:693–712. http://dx.doi.org/10.1016/S0006-3495(02)75432-5

McNew, J.A., H. Sondermann, T. Lee, M. Stern, and F. Brandizzi. 2013. GTP-dependent membrane fusion. *Annu. Rev. Cell Dev. Biol.* 29:529–550. http://dx.doi.org/10.1146/annurev-cellbio-101512-122328

Morin-Leisk, J., S.G. Saini, X. Meng, A.M. Makhov, P. Zhang, and T.H. Lee. 2011. An intramolecular salt bridge drives the soluble domain of GTP-bound atlastin into the postfusion conformation. *J. Cell Biol.* 195:605–615. http://dx.doi.org/10.1083/jcb.201105006

Moss, T.J., C. Andreazza, A. Verma, A. Daga, and J.A. McNew. 2011. Membrane fusion by the GTPase atlastin requires a conserved C-terminal cytoplasmic tail and dimerization through the middle domain. *Proc. Natl. Acad. Sci. USA.* 108:11133–11138. http://dx.doi.org/10.1073/pnas.1105056108

Mujumdar, R.B., L.A. Ernst, S.R. Mujumdar, C.J. Lewis, and A.S. Waggoner. 1993. Cyanine dye labeling reagents: Sulfoindocyanine succinimidyl esters. *Bioconjug. Chem.* 4:105–111. http://dx.doi.org/10.1021/bc00020a001

Orso, G., D. Pendin, S. Liu, J. Tosetto, T.J. Moss, J.E. Faust, M. Micaroni, A. Egorova, A. Martinuzzi, J.A. McNew, and A. Daga. 2009. Homotypic fusion of ER membranes requires the dynamin-like GTPase atlastin. *Nature.* 460:978–983. http://dx.doi.org/10.1038/nature08280

Park, S.H., and C. Blackstone. 2010. Further assembly required: Construction and dynamics of the endoplasmic reticulum network. *EMBO Rep.* 11:515–521. http://dx.doi.org/10.1038/embor.2010.92

Saini, S.G., C. Liu, P. Zhang, and T.H. Lee. 2014. Membrane tethering by the atlastin GTPase depends on GTP hydrolysis but not on forming the cross-over configuration. *Mol. Biol. Cell.* 25:3942–3953. http://dx.doi.org/10.1091/mbc.E14-08-1284

Skehel, J.J., and D.C. Wiley. 2000. Receptor binding and membrane fusion in virus entry: The influenza hemagglutinin. *Annu. Rev. Biochem.* 69:531–569. http://dx.doi.org/10.1146/annurev.biochem.69.1.531

Söllner, T.H. 2004. Intracellular and viral membrane fusion: A uniting mechanism. *Curr. Opin. Cell Biol.* 16:429–435. http://dx.doi.org/10.1016/j.ceb.2004.06.015

Stein, A., G. Weber, M.C. Wahl, and R. Jahn. 2009. Helical extension of the neuronal SNARE complex into the membrane. *Nature.* 460:525–528. http://dx.doi.org/10.1038/nature08156

Südhof, T.C., and J.E. Rothman. 2009. Membrane fusion: Grappling with SNARE and SM proteins. *Science.* 323:474–477. http://dx.doi.org/10.1126/science.1161748

Sutton, R.B., D. Fasshauer, R. Jahn, and A.T. Brunger. 1998. Crystal structure of a SNARE complex involved in synaptic exocytosis at 2.4 A resolution. *Nature.* 395:347–353. http://dx.doi.org/10.1038/26412

Tamm, L.K. 2003. Hypothesis: Spring-loaded boomerang mechanism of influenza hemagglutinin-mediated membrane fusion. *Biochim. Biophys. Acta.* 1614:14–23. http://dx.doi.org/10.1016/S0005-2736(03)00159-7

Tamm, L.K., J. Crane, and V. Kiessling. 2003. Membrane fusion: A structural perspective on the interplay of lipids and proteins. *Curr. Opin. Struct. Biol.* 13:453–466. http://dx.doi.org/10.1016/S0959-440X(03)00107-6

Weissenhorn, W., A. Carfí, K.H. Lee, J.J. Skehel, and D.C. Wiley. 1998. Crystal structure of the Ebola virus membrane fusion subunit, GP2, from the envelope glycoprotein ectodomain. *Mol. Cell.* 2:605–616. http://dx.doi.org/10.1016/S1097-2765(00)80159-8

Weissenhorn, W., A. Dessen, L.J. Calder, S.C. Harrison, J.J. Skehel, and D.C. Wiley. 1999. Structural basis for membrane fusion by enveloped viruses. *Mol. Membr. Biol.* 16:3–9. http://dx.doi.org/10.1080/096876899294706

Weissenhorn, W., A. Hinz, and Y. Gaudin. 2007. Virus membrane fusion. *FEBS Lett.* 581:2150–2155. http://dx.doi.org/10.1016/j.febslet.2007.01.093

Yersin, A., H. Hirling, P. Steiner, S. Magnin, R. Regazzi, B. Hüni, P. Huguenot, P. De los Rios, G. Dietler, S. Catsicas, and S. Kasas. 2003. Interactions between synaptic vesicle fusion proteins explored by atomic force microscopy. *Proc. Natl. Acad. Sci. USA*. 100:8736–8741. http://dx.doi.org/10.1073/pnas.1533137100

Zhao, X., D. Alvarado, S. Rainier, R. Lemons, P. Hedera, C.H. Weber, T. Tukel, M. Apak, T. Heiman-Patterson, L. Ming, et al. 2001. Mutations in a newly identified GTPase gene cause autosomal dominant hereditary spastic paraplegia. *Nat. Genet.* 29:326–331. http://dx.doi.org/10.1038/ng758